Microporous and Mesoporous Materials 239 (2017) 101–110

Contents lists available at ScienceDirect

Microporous and Mesoporous Materials

journal homepage: www.elsevier.com/locate/micromeso

An efficient catalyst of manganese supported on diatomite for toluene oxidation: Manganese species, catalytic performance, and structure-activity relationship

Peng Liu [a, d], Hongping He [a], Gaoling Wei [b], Dong Liu [a], Xiaoliang Liang [a, *], Tianhu Chen [c], Jianxi Zhu [a], Runliang Zhu [a]

[a] CAS Key Laboratory of Mineralogy and Metallogeny/Guangdong Provincial Key Laboratory of Mineral Physics and Materials, Guangzhou Institute of Geochemistry, Chinese Academy of Sciences, Guangzhou 510640, PR China
[b] Guangdong Institute of Eco-Environmental and Soil Sciences, Guangzhou 510650, PR China
[c] School of Resources and Environmental Engineering, Hefei University of Technology, Hefei 230009, PR China
[d] University of Chinese Academy of Sciences, Beijing 100049, PR China

ARTICLE INFO

Article history:
Received 27 July 2016
Received in revised form
28 September 2016
Accepted 28 September 2016
Available online 29 September 2016

Keywords:
Diatomite
Mn oxides
Catalytic oxidation
Toluene
TPSR

ABSTRACT

The work reports the preparation of diatomite-supported manganese catalysts by deposition-precipitation method, and their application for toluene oxidation. Microstructure and morphology of catalysts were investigated by Powder X-ray diffraction pattern (PXRD), thermogravimetric (TG), X-ray photoelectron spectroscopy (XPS), scanning electron microscopy (SEM), transmission electron microscopy (TEM) and nitrogen (N_2) adsorption-desorption isotherms. Temperature-programmed reduction (TPR) and temperature-programmed surface reaction (TPSR) were used to analyze the reducibility of Mn species and the reactivity of surface oxygen species, respectively. The characterization results reveal that the manganese species were mainly in the phase of amorphous MnO_2 and Mn_2O_3 on the diatomite, and the manganese species were successfully loaded on diatomite surface and filled in pores. With the increase of Mn content, the catalytic activity enhanced, due to the increase of surface oxygen species as adsorption-reaction sites. The Mn^{4+} played an important role in the superior catalytic activity towards toluene. The catalyst also displays high stability and superior activity towards toluene oxidation, which presents an applied interest. The effect of Mn content on the catalytic activity of catalysts was discussed in view of reaction mechanism and variations of physicochemistry properties.

1. Introduction

Toluene is an important organic solvent in the manufacture of dye, coating, rubber, and resin. Due to its low boiling point (111 °C), toluene can easily volatilize into air and become one of typical volatile organic compounds (VOCs). Toluene is hazardous to human health and environment. Long-term exposure to low concentration of toluene may result in serious chronic diseases, e.g., reproductive and teratology diseases [1], while inhaling high-level toluene in a short time would cause light-headedness, unconsciousness and even death [2]. Toluene in the atmosphere would transform into the precursor of photochemical ozone (O_3) and secondary organic aerosol, which are associated with photochemical smog and haze [3]. Thus, toluene in industrial waste gas must be effectively abated before its emission into atmosphere. Various techniques have been developed for the removal of gaseous toluene, e.g., adsorption, catalytic combustion, photocatalytic oxidation, plasma processing, and biological treatment [4]. Among them, catalytic combustion is regarded as an “end-of-pipe” technique, where toluene is destructed into CO_2 and H_2O over the catalysts at relatively low operation temperature (350–500 °C) [5], displaying a bright application prospect.

To achieve high efficiency for toluene removal and high selectivity of target products (CO_2 and H_2O, but no NO_x), the development of effective and efficient catalysts is particularly necessary. Currently, catalysts used for toluene oxidation are classified into two groups, namely, bulk or supported transition metal oxides [6], and supported noble metals [7]. Compared to supported noble

* Corresponding author.
E-mail address: liangxl@gig.ac.cn (X. Liang).

http://dx.doi.org/10.1016/j.micromeso.2016.09.053
1387-1811/

metal catalysts, transition metal oxide catalysts are more applicative, for their merits of low cost, high resistance to poisons, and thermal stability, though they are slightly less active in most cases [8].

Manganese oxides (MnO_x) including Mn_3O_4, Mn_2O_3, and MnO_2 are among the most active oxide catalysts for VOCs oxidation [9]. Manganese with electronic structure $3d^5 4s^2$ has variable oxidation states from −3 to +7. The presence of Mn^{2+}/Mn^{3+} or Mn^{3+}/Mn^{4+} redox couples and the active participation of lattice or surface oxygen in the manganese oxides facilitate the oxidation process through the Mars-Van Krevelen (MVK) mechanism [10]. In last decade, great efforts have been devoted to improving the catalytic activity of MnO_x by focusing on several fundamental constraint factors, e.g., valence, structure, morphology, and dispersion. For example, Ramesh et al. [11] reported that the reactivity shows an order of $MnO \leq MnO_2 < Mn_2O_3$ in the CO oxidation. MnO_x have various structures and morphology. Pyrolusite (β-MnO_2) with rutile-like structure is the most stable polymorph of MnO_2, while γ-MnO_2 has a highly disordered structure and is described as an intergrowth of elements of pyrolusite and ramsdelllite. But γ-MnO_2 is more suitable than β-MnO_2 for VOCs oxidation [12]. Si et al. prepared a high-efficiency γ-MnO_2 catalyst processing good catalytic performance in toluene oxidation [13]. The coupling of MnO_x with other metal oxides, e.g., Co_2O_3 [14], CuO [15], Fe_2O_3 [16], CeO_2 [17], is usually favorable for the catalytic performance. CeO_2 increases the oxygen storage capacity, while transition metal oxides improve the reducibility of composite. As large surface area assists in increasing the activity, microporous and mesoporus materials with large surface area, e.g., Al_2O_3 [18], anatase [19], zeolites [20], clays, and pillared clays [21,22], are used as excellent supports to make MnO_x nanoparticles well-dispersed. Materials with large surface area, abundant porosity, strong surface acidity, and high thermal stability, are proper supports for active species of VOCs oxidation [23]. However, the aforementioned catalysts have some disadvantages in practice, such as complicated preparation procedures or costly synthetic ingredients. A cheap and facile method for designing effective and efficient catalysts is still a desirable technical goal.

Diatomite, known as diatomaceous earth or kieselgur, is fine-grained and low-density biogenic sediment [24]. Diatomite frustules are mainly composed of amorphous hydrated silica ($SiO_2 \cdot nH_2O$), which is categorized as non-crystalline opal-A according to the mineralogical classification [25]. Diatomite is inexpensive and readily available, because diatomaceous silica is an abundant form of silica on earth and there are many diatomite reserves worldwide. With several unique physical and chemical characteristics, e.g., highly developed mesoporosity and/or macroporosity, strong acid resistance, thermal stability, and high mechanical strength, diatomite has a variety of applications, including as adsorbents, filters, fillers, catalysts supports, and adsorbents. Especially, the bimodal mesoporosity/macroporosity characteristic makes some diatomite exactly appropriate as adsorbent and support, because mesopores enhance specific surface area (SSA) and macropores increase the efficiency of the mass-transport and diffusion processes. From previous studies, naturally occurring and modified diatomite possessing good adsorptive properties has been successfully used for the adsorption of organic pollutants, e.g., benzene [24], toluene [26], dyes [27], and heavy metals, e.g., Cu(II) [25], Pb(II) [28], and Cr(VI) [29]. Based on above merits, diatomite was used as support for manganese oxides and applied in catalyst preparation for thermally oxidation of toluene in this study.

Herein, through the application of diatomite-supported manganese oxide as catalysts for thermally toluene oxidation, three aspects were focused on: (i) the valence, microstructure, and distribution of MnO_x on diatomite (ii) effect of supported MnO_x content on catalytic performance; (iii) the reaction mechanism, structure-activity relationship, and application prospect of the prepared catalyst. The fundamental information derived from this study is important for the application of diatomite as catalyst support and the development of novel catalysts for toluene abatement.

2. Materials and methods

2.1. Catalyst preparation

All the chemicals and reagents used in this study are of analytical grade. Raw diatomite sample from Changbai, Jilin Province, China, was purified using sedimentation method and denoted as Dt. The major elemental composition (wt%) determined by X-ray fluorescence analysis (XRF) is expressed as their corresponding oxides is SiO_2, 89.84%; Al_2O_3, 3.73%; K_2O, 0.77%; Fe_2O_3, 0.48%; Na_2O, 0.27%; TiO_2, 0.21%; MgO, 0.18%; CaO, 0.16%; MnO, 0.01%; P_2O_5, 0.01%; and ignition loss, 4.34%.

The diatomite-supported manganese species catalyst was prepared by the deposition-precipitation method. $Mn(NO_3)_2$ and $CO(NH_2)_2$ were added into 500 mL distilled water with mole ratio of 1:10, and then mixed with 10 g of Dt. The predetermined loading contents of Mn on Dt were 2.0%, 5.0%, 10.0%, and 20.0%. The solution was under stirring at 90 °C for 10 h. Then the particles were separated and washed until Mn^{2+} was completely removed in the supernatant. The obtained solid was dried at 80 °C overnight, pressed, crushed, and sieved to obtain particles with size of 0.25–0.50 mm. The particles were calcined at 400 °C in air for 2 h, predetermined calcination temperature to obtain catalyst with the best activity (Fig. A.1). To compare with the supported catalysts, the unsupported sample of $MnCO_3$ was prepared by above procedure except the addition of diatomite and calcination. The supported catalysts are labeled as Mn*x*-*T*, where *x* and *T* denote the determined Mn content and calcination temperature, respectively, while their precursors are labeled as Mn*x*.

2.2. Catalyst characterization

The Mn content on diatomite was determined by PerkinElmer AAnalyst 400 Flame Atomic Absorption Spectrometry. The carbon content was analyzed on a Vario EL III Elemental Analyzer with TCD detector. Powder X-ray diffraction (PXRD) patterns were recorded between 2° and 70° (2θ) at a step of 2° min^{-1} using a Bruker D8 advance diffractometer with Cu Kα radiation (40 kV and 40 mA). Thermogravimetric (TG) analyses were performed on a Netzsch STA 409 PC instrument under air atmosphere. The temperature increased from 30 to 400 °C at a rate of 10 °C min^{-1}, and kept at 400 °C for 2 h, and then increased from 400 °C to 1000 °C at a rate of 10 °C min^{-1}. Specific surface area (SSA) and porosity analysis were analyzed on the basis of N_2 adsorption-desorption isotherms at −196 °C with an ASAP 2020 instrument. All the samples were degassed at 150 °C for 12 h before test. Scanning electron microscopy (SEM) images were obtained using a ZEISS Supra 55 field emission scanning electron microscope in the high vacuum mode and with voltage of 30 kV. The samples were coated with a thin Au film to avoid charge accumulation on sample surface and improve image contrast. The linear scan of EDS was performed at voltage of 15 kV and operational height of 15 mm on EDAX TEAM affiliated to aforementioned SEM. Transmission electron microscopy (TEM) images were acquired using FEI Talos F200S instrument at an acceleration voltage of 200 kV. All particles were dispersed in ethanol on a carbon coated copper grid. X-ray photoelectron spectroscopy (XPS) analyses were performed on a Thermo Scientific K-Alpha instrument equipped with an Al Kα source (10 mA, 14 kV) and

operated at 1486.8 eV, and all binding energies were referenced to C 1s line at 284.8 eV. Temperature-programmed reduction (TPR) was carried out on Builder PCA-1200 equipped with TCD detector. The temperature was set in the range of 30–900 °C at a rate of 10 °C min^{-1}.

2.3. Toluene oxidation

The catalytic combustion of toluene was performed in a conventional fixed-bed reactor in the temperature range of 100–350 °C under atmospheric pressure. 200.0 mg of catalyst was loaded in a quartz tube reactor (i.d. = 6 mm) supported by a porous quartz plate. Gaseous toluene was generated by flowing N_2 into liquid toluene at 0 °C. The inlet gas composes of 1000 ppm toluene and 20 vol% oxygen balanced by N_2. The total flow rate was 100 mL min^{-1}, corresponding to gas hourly space velocity (GHSV) of 30 000 cm^3 g^{-1} h^{-1}. The concentration of toluene and CO_2 in effluent were analyzed on-line by a gas chromatograph (Agilent 7820A) equipped with FID detector, and a non-dispersive infrared CO_2 analyzer (Beijing Huayun GXH-3010E), respectively. No other chromatographic peak but that of toluene was detected in effluent. The temperature-programmed surface reactions (TPSR) experiments were also conducted. Toluene in N_2 was adsorbed in saturation on 200.0 mg of catalyst at 25 °C, followed by the introduction of N_2 (50 mL min^{-1}) to remove the residual toluene in apparatus for 1 h. Then the temperature was increased from 25 to 600 °C at 10 °C min^{-1}. The produced CO_2 was monitored online. Each experiment was repeated three times, and the error bar was set to standard deviation.

3. Results and discussion

3.1. Catalyst characterization

Chemical analysis results show that the Mn content on the prepared catalysts is 1.6%, 2.9%, 7.6%, and 14.1%, a bit lower than the theoretical content, 2.0%, 5.0%, 10.0%, and 20.0%, respectively, suggesting the incomplete precipitation of Mn cations on diatomite. Thus, the prepared catalysts are labeled as Mn1.6-400, Mn2.9-400, Mn7.6-400, and Mn14.1–400. As the Mn content is 2.9%, a little carbon is found in the catalyst of Mn2.9-400. The carbon content gradually increases with the increment of Mn content, indicating the incomplete decomposition of precursors.

In the PXRD patterns of purified diatomite (Fig. 1a), a broad low-intensity reflection centered at 21.6° appears in the range of 13–35°, which is characteristic of amorphous diatomaceous silica, accompanied with reflections at 20.8° and 26.6° related to quartz impurity (JCPDS No. 46-1045) [30]. With the increase of Mn content in the precursors, the intensity of reflections for $MnCO_3$ (JCPDS No. 86-0172) gradually increases. This indicates the main phase of $MnCO_3$ on the catalyst precursors, formed by the precipitation of Mn^{2+} and $CO(NH_2)_2$. After calcination at 400 °C, the reflections of $MnCO_3$ disappear except for Mn14.1–400 (Fig. 1b), illustrating the decomposition of $MnCO_3$ during calcination. For Mn14.1–400, besides the reflections of residual $MnCO_3$ and diatomite support, two weak reflections are found at 32.7° and 55.0°, ascribed to Mn_2O_3 (JCPDS No. 76-0150). But for most of diatomite-support Mn catalysts, no reflection related to Mn species exists. To verify the presence of Mn oxides on all the calcined samples, Mn7.6-400 was further calcined at 500, 600, 700, and 800 °C for 2 h. The reflections of Mn_2O_3 gradually increase in intensity with calcination temperature increase (Fig. A.2). This suggests the decomposition of most supported $MnCO_3$ to amorphous Mn oxides during calcination at 400 °C. However, the precursor of unsupported $MnCO_3$ after 400 °C calcination includes mainly $MnCO_3$ and a very small amount of Mn_2O_3 (Fig. 1b), in which the content ratio of $MnCO_3/Mn_2O_3$ is 18.2, obtained by K value method. It indicates that the decomposition temperature of $MnCO_3$ is higher than 400 °C. Thus, ascribed to dispersion of $MnCO_3$ by diatomite, the supported $MnCO_3$ has a lower decomposition temperature than that of unsupported $MnCO_3$.

To confirm the presence of amorphous Mn oxides on the catalysts, the calcination of precursors were investigated by TG. For $MnCO_3$ (Fig. A.3), the slow mass loss (about 2%) in TG curve at approximate 30–400 °C results from dehydration and dehydroxylation of $MnCO_3$ [31]. In the temperature range of 400–650 °C, a sharper mass loss with DTG peak appears approximately at 582 °C, corresponding to the multi-step decomposition of $MnCO_3 \rightarrow MnO_2 \rightarrow Mn_2O_3$. The mass loss about 31.7% during this decomposition matches well with the theoretical value (31.3%). Another mass loss of 1.3%, corresponding to a DTG peak at 885 °C, is ascribed to the transformation of Mn_2O_3 to Mn_3O_4 [32]. For the precursors (Fig. 2), besides the mass loss by dehydration and dehydroxylation in 30–400 °C, a proportion of mass loss is occurred during the heating at 400 °C for 2 h. This indicates that most $MnCO_3$ was decomposed during the calcination, consisting with the PXRD results. In Mn7.6 and Mn14.1, a mass loss less than 4% appears in 400–650 °C, increasing with the Mn content, ascribed to the decomposition of residual $MnCO_3$.

From the PXRD and TG analyses, $MnCO_3$, MnO_2, and Mn_2O_3 probably exist in the samples. Thus, XPS was carried out to study the composition of Mn species (Fig. 3). The binding energy of Mn 2p3/2 for as-prepared $MnCO_3$ is 641.7 eV, close to that of Mn^{3+} [33], but different from that of Mn^{4+} in range of 642.2–643.2 eV. Thus, the Mn 2p3/2 spectra can be deconvoluted into three components: i) Mn^{2+} of $MnCO_3$ and Mn^{3+} of Mn_2O_3 at 641.6–641.7 eV; ii) Mn^{4+} of amorphous MnO_2 at 643.2–643.5 eV; iii) shake-up satellite of Mn at 645.7–646.5 eV. Through the calculation of peak area, the

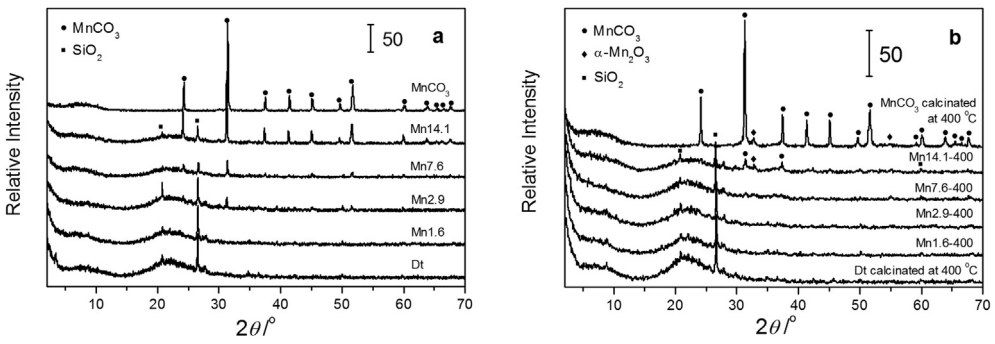

Fig. 1. The PXRD patterns of the prepared catalysts (b) and their precursors (a).

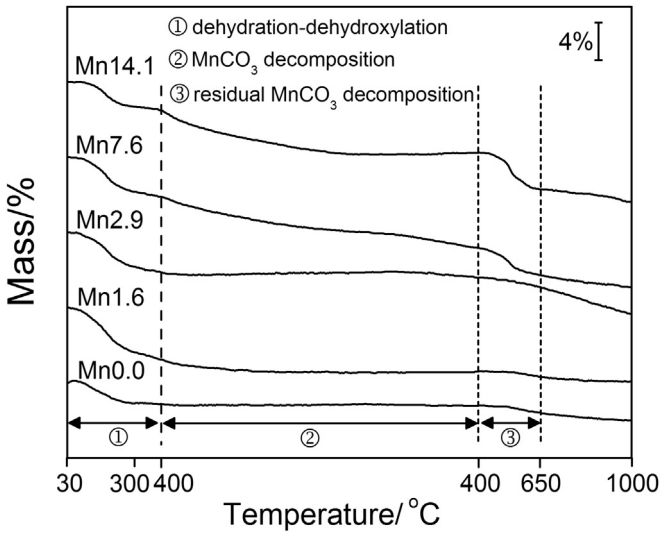

Fig. 2. The TG curves under air for the catalyst precursors.

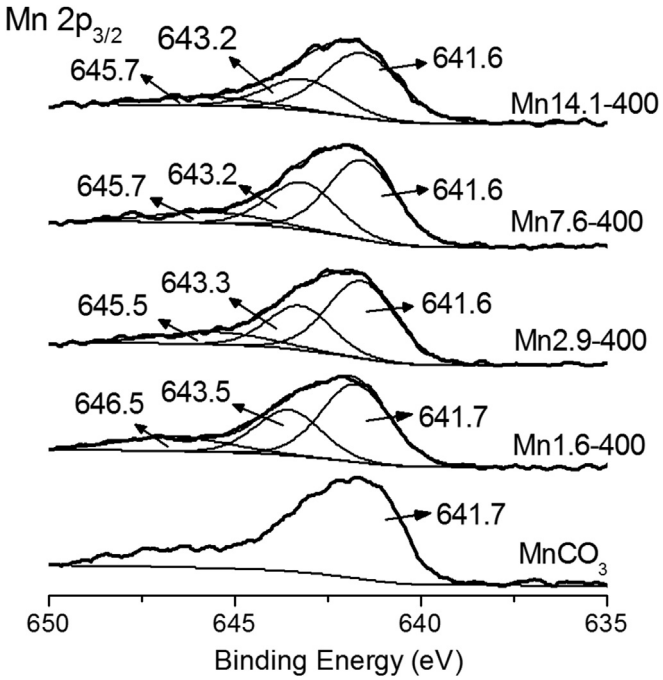

Fig. 3. The Mn $2p_{3/2}$ XPS spectra of diatomite-supported Mn catalysts and $MnCO_3$.

surface atomic ratio of $Mn^{4+}/(Mn^{3+}+Mn^{2+})$ is about 0.5. Based on the PXRD, TG, and XPS analyses, the main valence of Mn in the catalysts was +3 and +4. Moreover, the surface Mn/Si atomic ratio gradually increases from 0.082 (Mn1.6-400) to 0.101 (Mn7.6-400), but then decreases to 0.069 (Mn14.1–400). This is probably ascribed to the aggregation of Mn oxides on Mn14.1–400, suggesting the worse dispersion in the sample with high Mn content.

Due to the multivalence of Mn on the catalysts, TPR characterization was carried out to analyse the reducibility of prepared catalysts (Fig. 4). Since TCD detector was used to analyse the consumed H_2, the dehydration of catalyst in the temperature range of 30–150 °C was also sensitive, but did not overlap the reduction peaks of Mn species. For diatomite support and Mn1.6-400, the reduction by H_2 is quite subtle. With the increase of Mn content, the reduction peaks become obvious. Their TPR curves consist of two

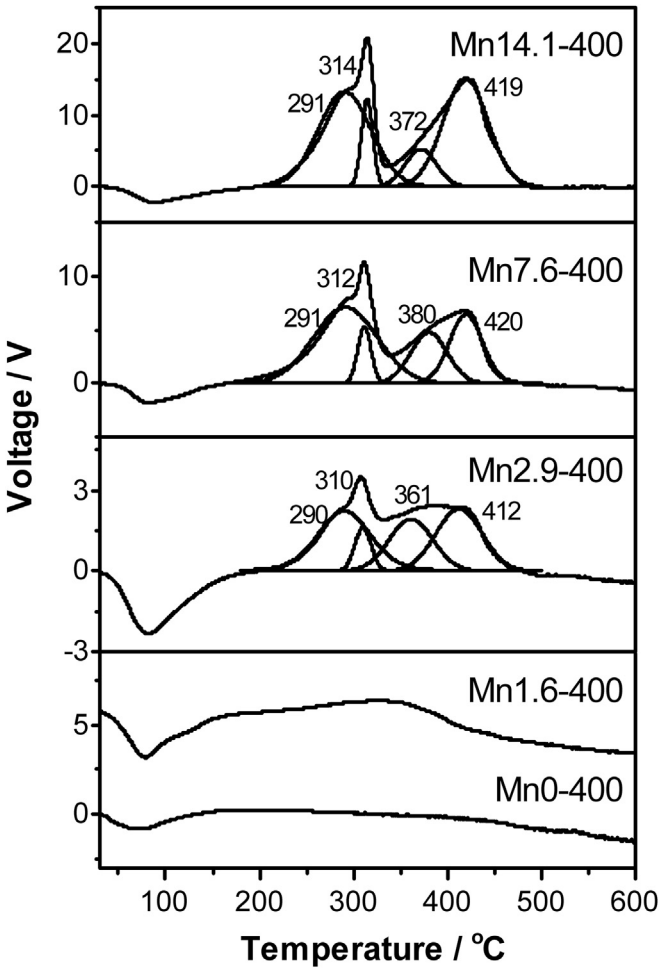

Fig. 4. The TPR curves of diatomite-supported Mn catalysts.

broad peaks, which are divided to four components. The first two components A and B with high intensity, at approximate 290 and 312 °C, are associated with the reduction of amorphous $MnO_2 \rightarrow Mn_2O_3 \rightarrow Mn_3O_4$, respectively [34,35]. The third component C at approximate 370 °C is probably related to the reduction of crystalline Mn_2O_3 to Mn_3O_4, whose reduction temperature is higher than that of amorphous Mn_2O_3. The last component at approximate 416 °C is attributed to the reduction of crystalline and amorphous Mn_3O_4 to MnO. Among the catalysts, the temperature of relevant reduction is identical, implying the similar lattice oxygen mobility. But the reduction peak area varies with the Mn contents (Table 1).

The morphology of diatomite and the supported Mn species was observed by SEM (Fig. 5). The calcined diatomite is in disc shape,

Table 1
The relative content of components, specific surface area and porous volume in diatomite-supported Mn catalysts.

Samples	C (wt%)	Mn (wt%)	[a]S_{BET} ($m^2\ g^{-1}$)	[b]V_T ($cm^3\ g^{-1}$)
Diatomite	0	0	21.0	0.048
Mn1.6-400	0	1.6	37.9	0.075
Mn2.9-400	0.04	2.9	36.3	0.076
Mn7.6-400	0.12	7.6	38.9	0.068
Mn14.1–400	0.50	14.1	33.0	0.063

[a]S_{BET}: Specific surface area.
[b]V_T: Total pore volume.

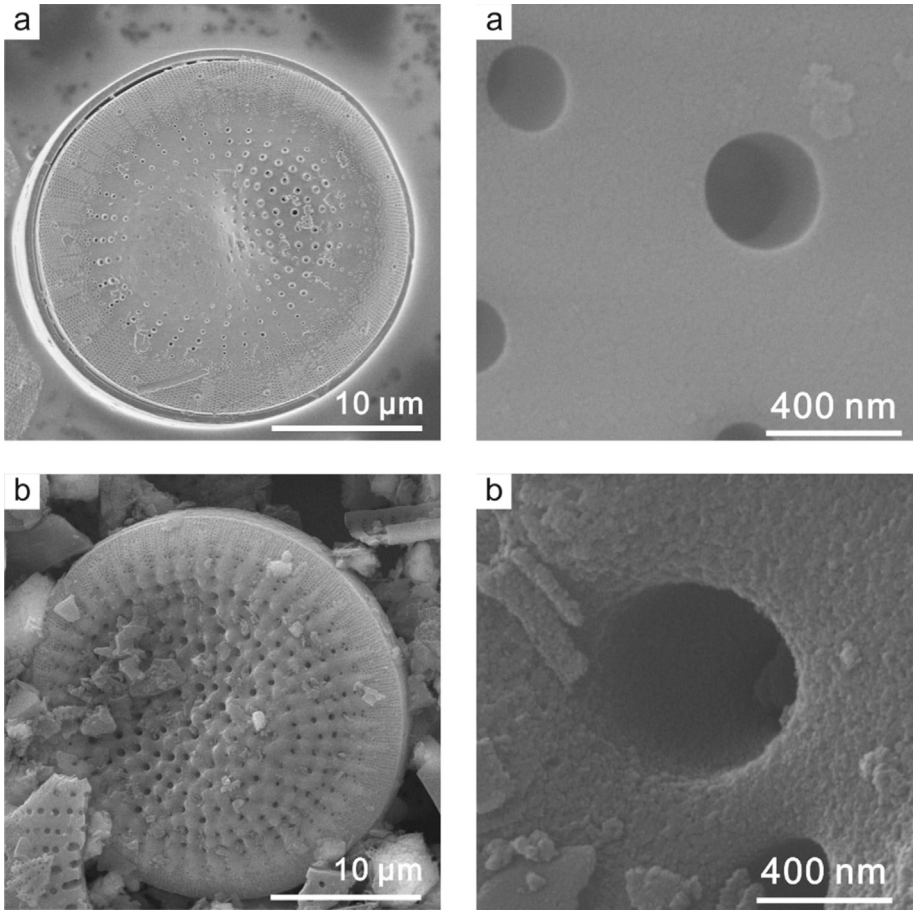

Fig. 5. The SEM images for calcined diatomite (a) and the catalyst of Mn14.1–400 (b).

with rich but irregular submicron pores. In the diatomite-supported Mn catalyst, Mn14.1–400, the diatomite surface becomes rough, indicating the successful loading of Mn species on diatomite. Most pores of the Mn-diatomite composite are still identifiable, which is beneficial for the transfer of reactants. However, the liner scan of EDS (Fig. A.4) shows that in Mn14.1–400, the Mn content of local position is significantly higher than those in adjacent area, ascribed to the existence of large Mn-containing particle. This phenomenon was not found in Mn7.6-400. It suggests that the dispersion of manganese species for Mn14.1–400 was not good as Mn7.6-400, in agreement with the Mn/Si in XPS analysis. The pore morphology was further examined by TEM (Fig. 6). For Mn2.9-400 and Mn7.6-400, most pores are occupied with aggregated particles but not completely blocking. The Mn oxide particles are well-dispersed in the pores, by forming some mesopores. However, some pores of Mn14.1–400 are completely filled by Mn oxide particles. This indicates that the dispersion of Mn species becomes less uniform in Mn14.1–400.

The nitrogen adsorption and desorption isotherms in all catalysts display typical characters of type II with H3 hysteresis loop (Fig. 7a), according to IUPAC-classification [36]. The sharp increase in nitrogen-adsorbed quantity near the relative pressure of 1.0 is ascribed to the presence of macropores in diatomite, in agreement with the SEM and TEM results. But the nitrogen-adsorbed quantity is quite low at relatively low pressure ($p/p0 < 0.1$), indicating the quite low micropores quantity [37]. According to the pore size distribution (PSD) curves (Fig. 7b), a broad peak related to mesopores is centered at 12 nm for calcined diatomite support, which becomes sharper and shifts approximately to 4 nm for the supported Mn catalysts. These mesopores originate from not only the mesopores on diatomite, but also the spaces between adjacent Mn oxide particles, since Mn oxides on the bulk surface of diatomite shell is non-porous, as observed from TEM. Moreover, the primary mesopores formed by manganese species on diatomite are smaller than that of $MnCO_3$ calcined at 400 °C, while the isotherms of diatomite-supported Mn catalysts are similar to that of calcined diatomite. Therefore, the Mn oxides are well-dispersed on diatomite. This fact is also evidenced by the results of SSA and porous volume (Table 2), which increase approximately 1.5 times after the loading of Mn oxides. Slight decrease of SSA and porous volume are seen in Mn14.1–400, ascribed to the aggregation of Mn oxide particles on diatomite.

3.2. Catalytic performance for toluene oxidation

The activity of diatomite-supported Mn catalysts for toluene oxidation is shown by the light-off curves as a function of temperature, 200–350 °C (Fig. 8a). To check if toluene was decomposed in thermal combustion, blank test was carried out on non-coated mesh in the reactor, where low toluene oxidation (<5%) was observed below 600 °C (not shown). The temperatures of 10% (T10), 50% (T50), and 90% (T90) toluene conversion as well as CO_2 generation are summarized in Table 3. The calcined diatomite support exhibits almost no catalytic activity for toluene oxidation. The catalytic activity gradually enhances as Mn content increases, with remarkable improvement from Mn1.6-400 to Mn7.6-400. But when the Mn content increases from 7.6% up to 14.1%, the increase of catalytic activity is less significant. This phenomenon is evidenced

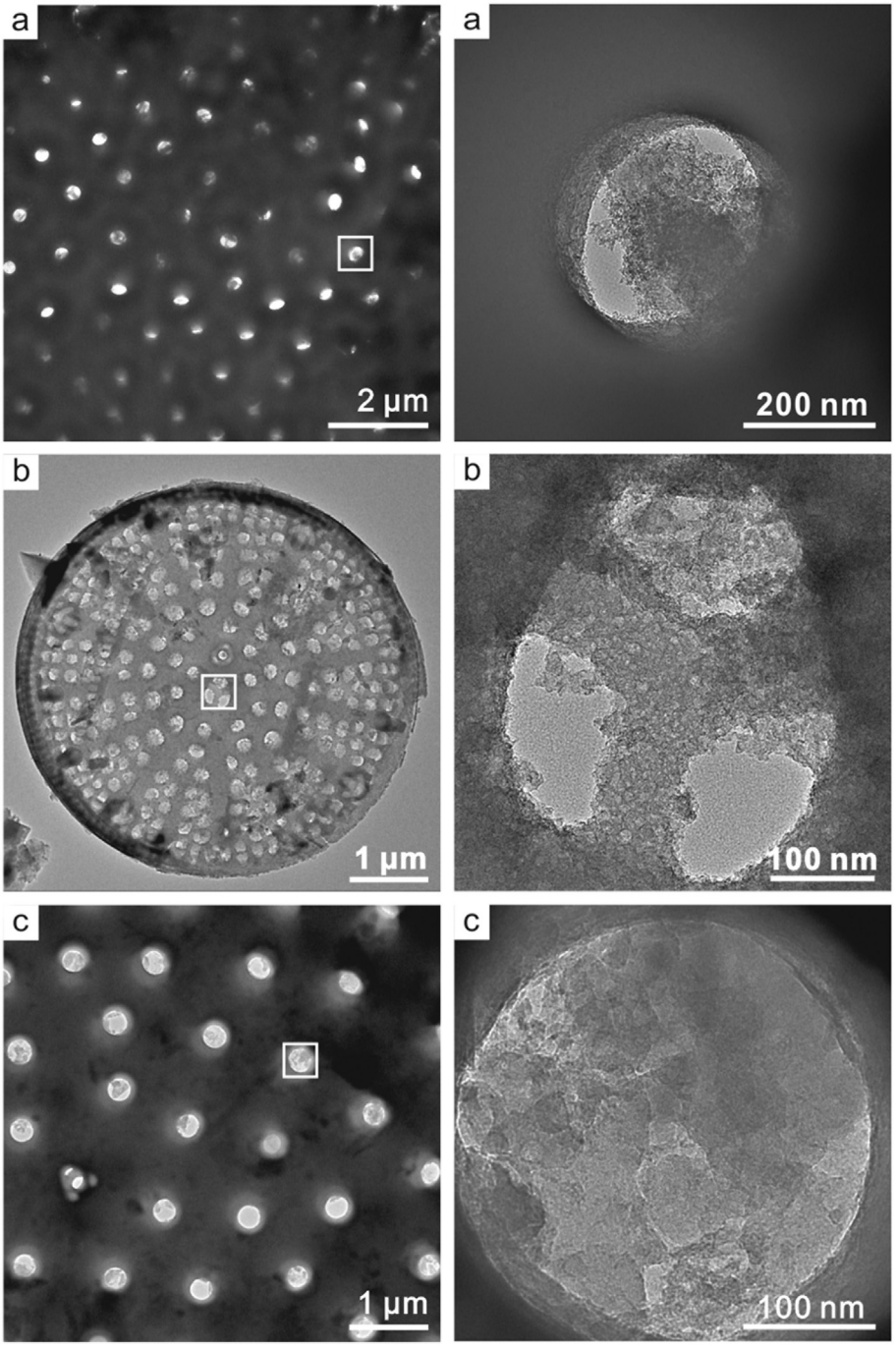

Fig. 6. The TEM images for catalyst samples of Mn2.9-400 (a), Mn7.6-400 (b) and Mn14.1–400 (c).

by the decrease of T90 in toluene conversion: Mn1.6-400 (higher than detection range) > Mn2.9-400 (314 °C) > Mn7.6-400 (274 °C) > Mn14.1–400 (267 °C).

To examine the catalytic selectivity for CO_2, the CO_2 generation during toluene oxidation was also traced (Fig. 8b). With the increase of Mn loading, the CO_2 generation curves distinctly shift to low temperature, indicating the enhancement of catalytic activity. The decrease of T10, T50, and T90 for CO_2 generation with the increase of Mn content is identical to those of toluene conversion. But CO_2 generation temperature is lower than that of toluene conversion. This indicates that toluene is not completely oxidized to CO_2 and H_2O. From previous studies [38,39], the byproducts in toluene oxidation include benzaldehyde, benzoic acid, and other oxygenated aromatic compounds. In 250–300 °C, the CO_2 generation rate is a bit lower than toluene conversion rate. For example, the CO_2 generation rate at 275 °C by Mn2.9-400, Mn7.6-400, and Mn14.1–400 are 10.1%, 53.0%, and 88.2%, respectively, slightly lower than their toluene conversion rates (22.1%, 94.9%, and 99.8%). But in 300–350 °C, the CO_2 generation rate by Mn7.6-400 and Mn14.1–400 is almost the same as toluene conversion rate, indicating the high selectivity to CO_2 of studied catalysts.

To investigate the effect of interaction between diatomite and manganese species on the catalytic activity of prepared catalysts, the reference samples were prepared by physically mixing

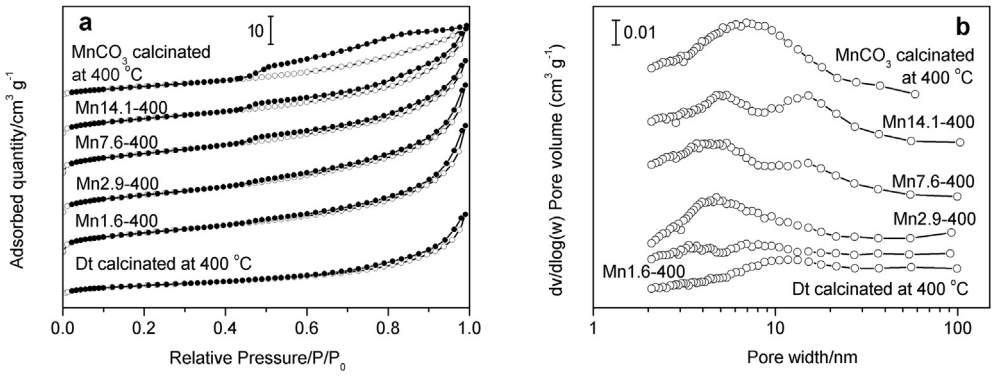

Fig. 7. The nitrogen absorption (open circle) and desorption (solid circle) isotherms (a) and pore size distributions (b) of diatomite-supported Mn catalysts and $MnCO_3$.

Table 2
The relative intensity of the reduction peaks on the TPR curves.

Sample	[a]Peak A	[b]Peak B	[c]Peak C	[d]Peak D
Mn2.9-400	37.5	7.6	24.4	30.5
Mn7.6-400	48.9	7.9	19.0	24.2
Mn14.1−400	41.7	8.3	9.6	40.4

[a]Peak A is ascribed to the reduction of amorphous MnO_2 to Mn_2O_3.
[b]Peak B is ascribed to the reduction of amorphous Mn_2O_3 to Mn_3O_4.
[c]Peak C is ascribed to the reduction of crystalline Mn_2O_3 to Mn_3O_4.
[d]Peak D is ascribed to the reduction of crystalline and amorphous Mn_3O_4 to MnO.

Table 3
Catalytic activity of diatomite-supported Mn catalysts for toluene oxidation and CO_2 generation.

Samples	Toluene conversion temperature/°C			CO_2 generation temperature/°C		
	[a]T10	[a]T50	[a]T90	[b]T10	[b]T50	[b]T90
Diatomite	–	–	–	–	–	–
Mn1.6-400	312	–	–	–	–	–
Mn2.9-400	258	287	314	275	308	348
Mn7.6-400	232	260	274	236	273	295
Mn14.1−400	215	242	267	226	259	279

[a]T10, [a]T50, and [a]T90 are ascribed to the temperature of 10%, 50%, and 90% toluene conversion, respectively.
[b]T10, [b]T50, and [b]T90 are ascribed to the temperature of 10%, 50%, and 90% CO_2 generation, respectively.
-: Out of the studied range.

diatomite and calcined $MnCO_3$ at 400 °C, and used as catalysts for toluene oxidation (Fig. A.5). The catalytic activities of reference samples were worse than that of the supported catalysts with same Mn content, e.g., Mn7.6-400 and Mn14.1−400. This indicates the important role of well-dispersion of Mn species on diatomite on the catalytic activity.

To evaluate the activity of diatomite-supported Mn catalysts, it is compared to the catalysts with Mn oxides loaded on other supports in toluene oxidation, reported by other groups (Table 4). The T90 by most listed catalysts vary in the temperature range of 200−450 °C, ascribed to various preparation methods, loading amount, support species, and reaction conditions. The T90 of Mn14.1−400 is lower or close to that of most reported catalysts. Moreover, diatomite is a kind of natural resource with low price, illustrating the promising application of diatomite as support for Mn oxide catalyst in toluene oxidation.

From previous studies, the catalytic oxidation of toluene over transition metal oxides follows the Mars-Van Krevelen (MVK) mechanism [40,41]. The reaction process includes the oxidation between toluene molecules and surface oxygen species, the reduction of oxidized catalyst by toluene, and the oxidation of catalyst by oxygen to form surface oxygen species. Temperature-programmed surface reaction (TPSR) experiment was performed without dioxygen to determine the nature of active sites, where absorbed toluene was reacted with surface oxygen under continuously increasing temperature (Fig. 9) [42]. The detection of CO_2 confirms that surface oxygen participates in toluene oxidation, and MVKs mechanism dominates in the reaction process. Few CO_2 was generated over calcined diatomite support and Mn1.6-400, due to the toluene desorption and their low catalytic activity. On Mn2.9-400, Mn7.6-400, and Mn14.1−400, three peaks appear. The first

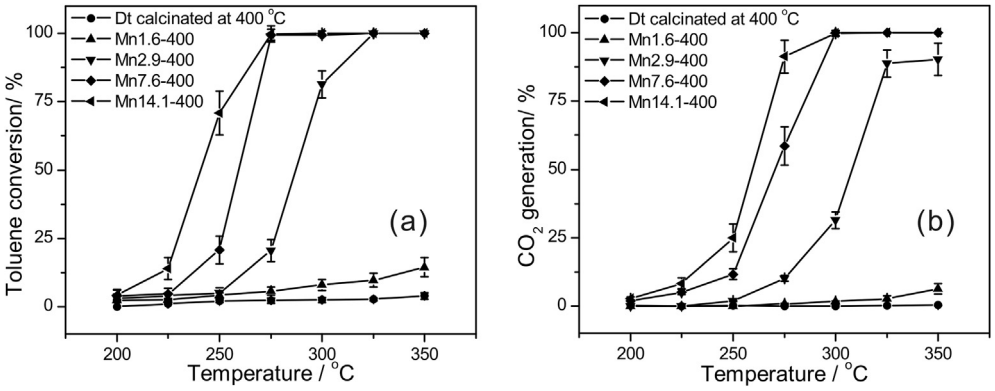

Fig. 8. The conversion curves of toluene oxidation and CO_2 generation over diatomite-supported Mn catalysts. Reaction conditions: [toluene] = 1000 ppm, [O_2] = 20%, catalyst mass = 200.0 mg, total flow rate = 100 mL min^{-1} and GHSV = 30 000 cm^3 g^{-1} h^{-1}.

Table 4
Main data of research papers on the oxidation of toluene over manganese oxides supported on different supports.

Supports	Loading amount	Surface area/$m^2\ g^{-1}$	Concentration/ppm	GHSV	Conversion of T90/°C	Ref.
α-Al_2O_3	9.4 wt%	15	1000	15000 h^{-1}	289	[44]
ZrO_2	9.4 wt%	21	1000	15000 h^{-1}	*	[44]
SiO_2	9.4 wt%	280	1000	15000 h^{-1}	441	[44]
θ-δ-Al_2O_3	11.3 wt%	103	5000	20000 $cm^3\ g^{-1}\ h^{-1}$	364	[18]
γ-Al_2O_3	15.0 wt%	62	1000	30000 $cm^3\ g^{-1}\ h^{-1}$	338	[45]
TiO_2	15.0 wt%	9	1000	30000 $cm^3\ g^{-1}\ h^{-1}$	439	[45]
SBA-15	10.0 wt%	618	1600	21000 h^{-1}	314	[46]
Zeolite	9.5 wt%	54	1000	15000 h^{-1}	297	[47]
Apatite	10.0 wt%	76	800	30000 $cm^3\ g^{-1}\ h^{-1}$	210	[48]
Diatomite	7.6 wt%	33	1000	30000 $cm^3\ g^{-1}\ h^{-1}$	294	This study

*Not reaching the studied range.

two peaks in 200–370 °C are related the adsorption-oxidation sites, i.e., surface lattice oxygen (O^{2-}) and adsorbed oxygen (HO−). The CO_2 amount produced in toluene oxidation is related to the availability of surface oxygen. On the catalyst containing more Mn, more CO_2 was generated, and CO_2 generation peaks shifts to low temperature. This indicates the toluene oxidation on diatomite-supported Mn catalysts followed the MVKs mechanism, improved with the increase of Mn content. For Mn2.9-400, Mn7.6-400, and Mn14.1–400, the total CO_2 produced amount for these two peaks was 16.3, 20.5, and 30.0 μmol g^{-1} cat. The last peak in 420–600 °C was ascribed to the decomposition of $MnCO_3$, in agreement with the results of PXRD and TG that the intensity increases with Mn content.

3.3. Structure-reactivity relationship

Based on the MVKs mechanism, the activity of diatomite-supported Mn catalysts for toluene oxidation is probably related to several factors, i.e., specific surface area, surface oxygen species, and the reducibility of Mn oxides. In this study, surface oxygen species was positively related to the intensity of CO_2 peak in TPSR reaction, where CO_2 was generated in the toluene oxidation by surface oxygen on the catalysts. Mn reduction intensity is related to the intensity of peak area of TPR curves. More bulk oxygen can be reduced, resulting in more lattice oxygen involved in the oxidation. The reduction temperatures of Mn^{4+} and Mn^{3+} center at approximate 290 and 312 °C, which are in the reaction temperature range of 250–350 °C. But the intensity of reduction peak of Mn^{4+} is much larger than that of Mn^{3+}. Higher oxidation state of Mn species is preferable for oxidation reactions over the manganese-containing catalysts. Thus, the reducibility of studied catalysts during the reaction mainly depends on the Mn^{4+} reducibility.

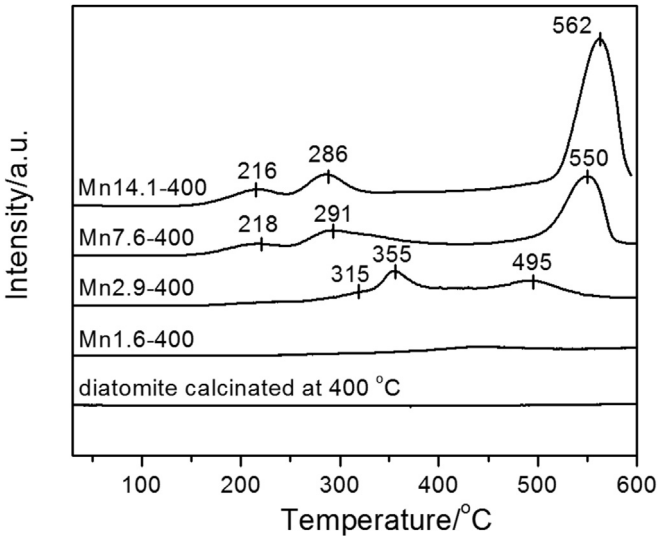

Fig. 9. The CO_2 generation in the temperature-programmed surface reaction (TPSR) between toluene and diatomite-supported Mn catalysts.

From the catalytic oxidation of toluene, the catalytic activity gradually enhances with the Mn content increase, but the enhancement is less significant at high Mn content. The reduction temperature of Mn^{4+} for Mn2.9-400, Mn7.6-400, and Mn14.1–400 is similar, indicating the reduction temperature is not the constraint factor. The decrease of enhancement can be related to the decrease of relative intensity of amorphous MnO_2, as shown in Table 2. For diatomite and Mn1.6-400, although their SSA value is large (Table 1), the reduction signal of Mn oxides (Fig. 9) and CO_2 amount generated in TPSR reaction are quite low, indicating their low Mn content and surface site intensity. The TPR curve of Mn1.6-400 also shows low reduction intensity of bulk oxygen. These well explain their worse catalytic activity. For the catalysts with relatively high Mn content, i.e., Mn2.9-400, Mn7.6-400, and Mn14.1–400, they display enhanced reactivity for toluene oxidation, with the increase of Mn content. This is probably ascribed to the increase of surface oxygen and reduction intensity of Mn oxides, which supplies more oxygen and facilitates the redox cycle in catalytic reaction, respectively [43]. But from N_2 adsorption-desorption, SEM, and TEM characterizations, the increase of Mn content results in the particle aggregation and the decrease of SSA and pore volume. Moreover, the relative content of residual $MnCO_3$ also gradually increases. These two variations probably lead to the insignificant improvement of catalytic activity over Mn14.1–400.

3.4. Catalytic stability and moisture effect

Catalytic stability is critical for the application of catalysts. In this study, a lifetime test was carried out over Mn14.1–400 at 325 °C for a week (Fig. 10). In the initial three days, the catalytic activity achieved complete CO_2 generation steadily. However, sharp increase of CO_2 over 100% appeared in the last four days, and became more frequently as the reaction continued. After lifetime test, the catalyst was recycled for toluene oxidation, and it showed slightly worse catalytic activity than the fresh catalyst. The PXRD pattern of the recycled Mn14.1–400 shows the disappearance of $MnCO_3$ and the increase of Mn_2O_3 (Fig. A.6). Thus, the sharp increase of CO_2 is derived from the decomposition of residual $MnCO_3$. The deactivation of catalyst is attributed to formation of more Mn_2O_3. But the catalytic activity of the recycled Mn14.1–400 is still superior above 300 °C (Fig. A.7).

Besides catalytic stability, the resistance to water is also important for application of catalysts in VOCs oxidation. The effect of water on the catalytic oxidation of toluene over Mn14.1–400 was

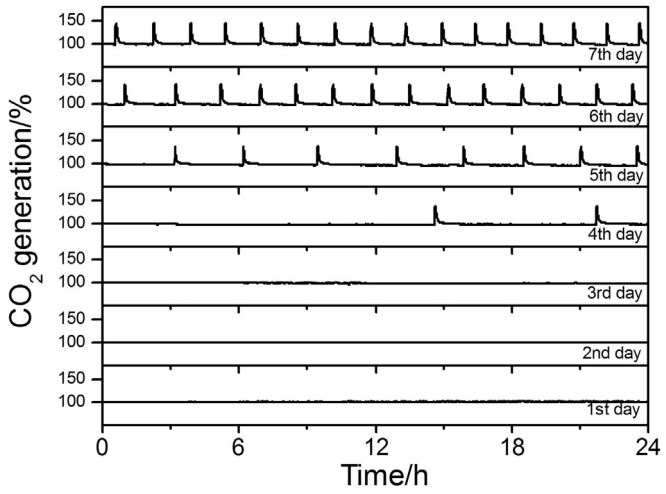

Fig. 10. Long term stability of Mn14.1–400 catalyst at 325 °C. Reaction conditions: [toluene] = 1000 ppm, [O_2] = 20%, catalyst mass = 200.0 mg, total flow rate = 100 mL min^{-1} and GHSV = 30 000 cm^3 g^{-1} h^{-1}.

investigated by adding 5000 ppm water to the feed gas at 325 °C with GHSV of 30 000 and 300 000 cm^3 g^{-1} h^{-1} (Fig. 11). At the GHSV of 3 × 10^4 cm^3 g^{-1} h^{-1}, the moisture did not affect the catalytic performance of catalyst. The addition of water caused only a slight decrease in CO_2 generation at GHSV of 3 × 10^5 cm^3 g^{-1} h^{-1}, but immediately recovered after the water introduction stopped. This indicates that the diatomite-supported Mn catalysts are not so sensitive to the presence of moisture at high temperature, unlike previously reported noble metal catalysts.

4. Conclusions

In this work, the catalytic oxidation of toluene over manganese-supported on diatomite catalysts was studied. The following findings can be derived from the present investigation, which might be beneficial for the application of natural diatomite and the development of catalysts for VOC elimination.

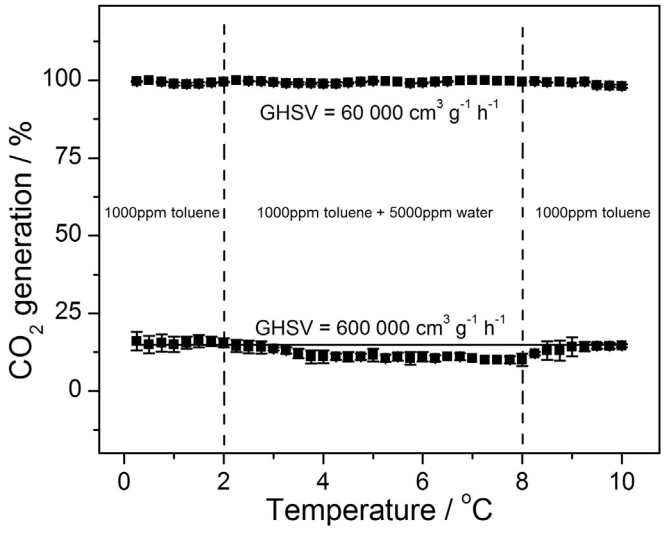

Fig. 11. Effect of moisture on toluene oxidation over the Mn14.1–400 catalyst with GHSV of 30 000 and 300 000 cm^3 g^{-1} h^{-1} at 325 °C. Reaction conditions: [toluene] = 1000 ppm, [O_2] = 20%, catalyst mass = 200 and 20 mg, [H_2O] = 5000 ppm, total flow rate = 100 mL min^{-1} and GHSV = 30 000 and 300 000 cm^3 g^{-1} h^{-1}.

(i) The manganese species are mainly in the phase of amorphous MnO_2 and Mn_2O_3 on the diatomite, accompanied with low content of $MnCO_3$. The Mn oxides gradually aggregate on diatomite as the increase of Mn content.

(ii) The manganese-supported on diatomite catalysts show excellent activity and high selectivity to CO_2 for toluene oxidation. With the increase of Mn content, the catalytic activity becomes better. The catalysts also show high activity toward toluene oxidation even after a week of test, indicating strong stability.

(iii) The reaction mechanism in this study follows the Mars-Van Krevelen (MVK) mechanism. With higher adsorption-reaction sites associated with surface oxygen, the catalytic activity of manganese-supported on diatomite catalysts improves. Moreover, the superior catalytic activity is ascribed to the excellent reducibility of Mn^{4+}.

Acknowledgement

This is contribution No.IS-2301 from GIGCAS. This work was financially supported by the National Natural Science Foundation of China (Grant No. 41572032), Natural Science Foundation for Distinguished Young Scientists of Guangdong Province (Grant No. 2016A030306034), Natural Science Foundation of Guangdong Province, China (Grant No. S2013030014241), Special Project on the Integration of Industry, Education and Research of Guangdong Province (Grant No. 2013B091500077), Youth Innovation Promotion Association CAS (Grant No. 2014324), and CAS/SAFEA International Partnership Program for Creative Research Teams (Grant No. 20140491534).

Appendix A. Supplementary data

Supplementary data related to this article can be found at http://dx.doi.org/10.1016/j.micromeso.2016.09.053.

References

[1] J.H. Hannigan, S.E. Bowen, Reproductive toxicology and teratology of abused toluene, Syst. Biol. Reprod. Med. 56 (2010) 184–200.
[2] D.J. Hsu, H.L. Huang, H.Y. Lin, T.S. Lin, Potential volatile organic compound exposure from dry process photocopiers in operation-idle mode, Bull. Eng. Geol. Environ. 76 (2006) 922–929.
[3] J. Williams, R. Koppmann, in: Koppman (Ed.), Volatile Organic Compounds in the Atmosphere: an Overview, Volatile Organic Compounds in the Atmosphere, 2007, pp. 1–32.
[4] G.R. Parmar, N.N. Rao, Emerging Control technologies for volatile organic compounds, Crit. Rev. Environ. Sci. Technol. 39 (2009) 41–78.
[5] K. Everaert, J. Baeyens, Catalytic combustion of volatile organic compounds, J. Hazard. Mater. 109 (2004) 113–139.
[6] S.A.C. Carabineiro, X. Chen, M. Konsolakis, A.C. Psarras, P.B. Tavares, J.J.M. Orfao, M.F.R. Pereira, J.L. Figueiredo, Catalytic oxidation of toluene on Ce-Co and La-Co mixed oxides synthesized by exotemplating and evaporation methods, Catal. Today 244 (2015) 161–171.
[7] Y.T. Lai, T.C. Chen, Y.K. Lan, B.S. Chen, J.H. You, C.M. Yang, N.C. Lai, J.H. Wu, C.S. Chen, Pt/SBA-15 as a highly efficient catalyst for catalytic toluene oxidation, ACS Catal. 4 (2014) 3824–3836.
[8] W. Li, J. Wang, H. Gong, Catalytic combustion of VOCs on non-noble metal catalysts, Catal. Today 148 (2009) 81–87.
[9] S.C. Kim, W.G. Shim, Catalytic combustion of VOCs over a series of manganese oxide catalysts, Appl. Catal. B 98 (2010) 180–185.
[10] A.R. Gandhe, J.S. Rebello, J.L. Figueiredo, J.B. Fernandes, Manganese oxide OMS-2 as an effective catalyst for total oxidation of ethyl acetate, Appl. Catal. B 72 (2007) 129–135.
[11] K. Ramesh, L.W. Chen, F.X. Chen, Y. Liu, Z. Wang, Y.F. Han, Re-investigating the CO oxidation mechanism over unsupported MnO, Mn_2O_3 and MnO_2 catalysts, Catal. Today 131 (2008) 477–482.
[12] L. Lamaita, M.A. Peluso, J.E. Sambeth, H.J. Thomas, Synthesis and characterization of manganese oxides employed in VOCs abatement, Appl. Catal. B 61 (2005) 114–119.
[13] W.Z. Si, Y. Wang, Y. Peng, X. Li, K.Z. Li, J.H. Li, A high-efficiency gamma-MnO_2-like catalyst in toluene combustion, Chem. Commun. 51 (2015) 14977–14980.

[14] D.A. Aguilera, A. Perez, R. Molina, S. Moreno, Cu-Mn and Co-Mn catalysts synthesized from hydrotalcites and their use in the oxidation of VOCs, Appl. Catal. B 104 (2011) 144–150.
[15] V.H. Vu, J. Belkouch, A. Ould-Dris, B. Taouk, Removal of hazardous chlorinated VOCs over Mn-Cu mixed oxide based catalyst, J. Hazard. Mater. 169 (2009) 758–765.
[16] P. Liu, H.P. He, G.L. Wei, X.L. Liang, F.H. Qi, F.D. Tan, W. Tan, J.X. Zhu, R.L. Zhu, Effect of Mn substitution on the promoted formaldehyde oxidation over spinel ferrite: catalyst characterization, performance and reaction mechanism, Appl. Catal. B 182 (2016) 476–484.
[17] D. Delimaris, T. Ioannides, VOC oxidation over MnO_x-CeO_2 catalysts prepared by a combustion method, Appl. Catal. B 84 (2008) 303–312.
[18] F.N. Aguero, B.P. Barbero, L. Gambaro, L.E. Cadus, Catalytic combustion of volatile organic compounds in binary mixtures over MnO_x/Al_2O_3 catalyst, Appl. Catal. B 91 (2009) 108–112.
[19] Y. Liu, M.F. Luo, Z.B. Wei, Q. Xin, P.L. Ying, C. Li, Catalytic oxidation of chlorobenzene on supported manganese oxide catalysts, Appl. Catal. B 29 (2001) 61–67.
[20] W.B. Li, M. Zhuang, T.C. Xiao, M.L.H. Green, MCM-41 supported Cu-Mn catalysts for catalytic oxidation of toluene at low temperatures, J. Phys. Chem. B 110 (2006) 21568–21571.
[21] L.M. Gandia, M.A. Vicente, A. Gil, Complete oxidation of acetone over manganese oxide catalysts supported on alumina- and zirconia-pillared clays, Appl. Catal. B 38 (2002) 295–307.
[22] T. Mishra, P. Mohapatra, K.M. Parida, Synthesis, characterisation and catalytic evaluation of iron-manganese mixed oxide pillared clay for VOC decomposition reaction, Appl. Catal. B 79 (2008) 279–285.
[23] H.B. Huang, Y. Xu, Q.Y. Feng, D.Y.C. Leung, Low temperature catalytic oxidation of volatile organic compounds: a review, Catal. Sci. Technol. 5 (2015) 2649–2669.
[24] W.B. Yu, L.L. Deng, P. Yuan, D. Liu, W.W. Yuan, P. Liu, H.P. He, Z.H. Li, F.R. Chen, Surface silylation of natural mesoporous/macroporous diatomite for adsorption of benzene, J. Colloid. Interf. Sci. 448 (2015) 545–552.
[25] P. Yuan, D. Liu, M. Fan, D. Yang, R. Zhu, F. Ge, J. Zhu, H. He, Removal of hexavalent chromium [Cr(VI)] from aqueous solutions by the diatomite-supported/unsupported magnetite nanoparticles, J. Hazard. Mater. 173 (2010) 614–621.
[26] M. Aivalioti, P. Papoulias, A. Kousaiti, E. Gidarakos, Adsorption of BTEX, MTBE and TAME on natural and modified diatomite, J. Hazard. Mater. 207 (2012) 117–127.
[27] Z. Al-Qodah, W.K. Lafi, Z. Al-Anber, M. Al-Shannag, A. Harahsheh, Adsorption of methylene blue by acid and heat treated diatomaceous silica, Desalination 217 (2007) 212–224.
[28] G.D. Sheng, S.W. Wang, J. Hu, Y. Lu, J.X. Li, Y.H. Dong, X.K. Wang, Adsorption of Pb(II) on diatomite as affected via aqueous solution chemistry and temperature, Colloid Surf. A 339 (2009) 159–166.
[29] P. Yuan, D. Liu, M.D. Fan, D. Yang, R.L. Zhu, F. Ge, J.X. Zhu, H.P. He, Removal of hexavalent chromium [Cr(VI)] from aqueous solutions by the diatomite-supported/unsupported magnetite nanoparticles, J. Hazard. Mater. 173 (2010) 614–621.
[30] Z.M. Sun, S.L. Zheng, G.A. Ayoko, R.L. Frost, Y.F. Xi, Degradation of simazine from aqueous solutions by diatomite-supported nanosized zero-valent iron composite materials, J. Hazard. Mater. 263 (2013) 768–777.
[31] R. Giovanoli, Thermogravimetry of manganese dioxides, Thermochim. Acta 234 (1994) 303–313.
[32] L. Liu, Z.J. Yang, H. Liang, H.X. Yang, Y.Z. Yang, Facile synthesis of $MnCO_3$ hollow dumbbells and their conversion to manganese oxide, Mater. Lett. 64 (2010) 2060–2063.
[33] K.H. Park, S.M. Lee, S.S. Kim, D.W. Kwon, S.C. Hong, Reversibility of Mn valence state in MnO_x/TiO_2 catalysts for low-temperature selective catalytic reduction for NO with NH_3, Catal. Lett. 143 (2013) 246–253.
[34] P.R. Ettireddy, N. Ettireddy, S. Mamedov, P. Boolchand, P.G. Smirniotis, Surface characterization studies of TiO_2 supported manganese oxide catalysts for low temperature SCR of NO with NH_3, Appl. Catal. B 76 (2007) 123–134.
[35] E. Stobbe, B. De Boer, J. Geus, The reduction and oxidation behaviour of manganese oxides, Catal. Today 47 (1999) 161–167.
[36] M. Thommes, K. Kaneko, A.V. Neimark, J.P. Olivier, F. Rodriguez-Reinoso, J. Rouquerol, K.S. Sing, Physisorption of gases, with special reference to the evaluation of surface area and pore size distribution (IUPAC Technical Report), Pure Appl. Chem. 87 (2015) 1051–1069.
[37] N. van Garderen, F.J. Clemens, J. Kaufmann, M. Urbanek, M. Binkowski, T. Graule, C.G. Aneziris, Pore analyses of highly porous diatomite and clay based materials for fluidized bed reactors, Microporous Mesoporous Mater. 151 (2012) 255–263.
[38] R. Mendez-Roman, N. Cardona-Martınez, Relationship between the formation of surface species and catalyst deactivation during the gas-phase photocatalytic oxidation of toluene, Catal. Today 40 (1998) 353–365.
[39] A.P. Antunes, M.F. Ribeiro, J.M. Silva, F.R. Ribeiro, P. Magnoux, M. Guisnet, Catalytic oxidation of toluene over CuNaHY zeolites - Coke formation and removal, Appl. Catal. B 33 (2001) 149–164.
[40] C. Doornkamp, V. Ponec, The universal character of the Mars and Van Krevelen mechanism, J. Mol. Catal. A Chem. 162 (2000) 19–32.
[41] U. Menon, V.V. Galvita, G.B. Marin, Reaction network for the total oxidation of toluene over CuO-CeO_2/Al_2O_3, J. Catal. 283 (2011) 1–9.
[42] V.P. Santos, M.F.R. Pereira, J.J.M. Orfao, J.L. Figueiredo, The role of lattice oxygen on the activity of manganese oxides towards the oxidation of volatile organic compounds, Appl. Catal. B 99 (2010) 353–363.
[43] X.F. Tang, Y.G. Li, X.M. Huang, Y.D. Xu, H.Q. Zhu, J.G. Wang, W.J. Shen, MnOx-CeO_2 mixed oxide catalysts for complete oxidation of formaldehyde: effect of preparation method and calcination temperature, Appl. Catal. B 62 (2006) 265–273.
[44] G.S. Pozan, Effect of support on the catalytic activity of manganese oxide catalysts for toluene combustion, J. Hazard. Mater. 221 (2012) 124–130.
[45] S.C. Jung, Y.K. Park, H.Y. Jung, U.I. Kang, J.W. Nah, S.C. Kim, Effects of calcination and support on supported manganese catalysts for the catalytic oxidation of toluene as a model of VOCs, Res. Chem. Intermed. 42 (2016) 185–199.
[46] Z.P. Qu, Y.B. Bu, Y. Qin, Y. Wang, Q. Fu, The effects of alkali metal on structure of manganese oxide supported on SBA-15 for application in the toluene catalytic oxidation, Chem. Eng. J. 209 (2012) 163–169.
[47] G.S.P. Soylu, Z. Ozcelik, I. Boz, Total oxidation of toluene over metal oxides supported on a natural clinoptilolite-type zeolite, Chem. Eng. J. 162 (2010) 380–387.
[48] D. Chlala, J.M. Giraudon, N. Nuns, C. Lancelot, R.N. Vannier, M. Labaki, J.F. Lamonier, Active Mn species well dispersed on Ca^{2+} enriched apatite for total oxidation of toluene, Appl. Catal. B 184 (2016) 87–95.